SEISMOLOGY

Missing link between the Hayward and Rodgers Creek faults

Janet Watt,[1]* David Ponce,[2] Tom Parsons,[2] Patrick Hart[1]

The next major earthquake to strike the ~7 million residents of the San Francisco Bay Area will most likely result from rupture of the Hayward or Rodgers Creek faults. Until now, the relationship between these two faults beneath San Pablo Bay has been a mystery. Detailed subsurface imaging provides definitive evidence of active faulting along the Hayward fault as it traverses San Pablo Bay and bends ~10° to the right toward the Rodgers Creek fault. Integrated geophysical interpretation and kinematic modeling show that the Hayward and Rodgers Creek faults are directly connected at the surface—a geometric relationship that has significant implications for earthquake dynamics and seismic hazard. A direct link enables simultaneous rupture of the Hayward and Rodgers Creek faults, a scenario that could result in a major earthquake (M = 7.4) that would cause extensive damage and loss of life with global economic impact.

INTRODUCTION

The Hayward-Rodgers Creek fault zone cuts through the heart of the urban San Francisco Bay Area (Fig. 1), which boasts the fourth largest economy in the United States and ranks among the top 20 in the world. Recent constraints show that the length of a combined Hayward-Rodgers Creek fault zone is ~190 km, extending from Alum Rock in the south (*1*) to just north of Healdsburg (*2*). The ability of an earthquake on the Hayward fault to continue onto its northern extension along the Rodgers Creek fault (or vice versa) greatly depends on the geometrical relationship between these faults beneath San Pablo Bay.

The Hayward-Rodgers Creek fault zone is considered the most likely bay area fault to experience an earthquake with moment magnitude (M) of ≥6.7 within the next 30 years (*3*), yet the location and connectivity of the Hayward and Rodgers Creek faults remain uncertain beneath San Pablo Bay. Where the faults enter the bay, their projections are separated across-strike by ~5 km. The Hayward and Rodgers Creek faults either are parallel and separated by a 4- to 6-km-wide gap or "stepover" (*4*–*6*) or join up as a throughgoing fault bend (*7*–*10*) beneath San Pablo Bay. Neither of these interpretations has been supported by direct observations of near-surface, active faulting. The shallow water depth (<2 m) and widespread gas in the bay sediments make acoustic imaging of the submerged geologic structure difficult, which may partially explain why the geometry of the Hayward and Rodgers Creek faults here has remained a mystery for so long.

Resolving this uncertainty is particularly important because the alternative fault models (fault stepover versus fault bend) have different implications for earthquake hazard. Fault connectivity defines the maximum earthquake rupture length, and the three-dimensional (3D) geometry of faults affects the dynamics of fault rupture, slip, and ground motion (*11*–*15*). Details of the 3D fault geometry at stepovers and bends—particularly in urban settings—are often lacking, limiting efforts to constrain hazard calculations in these areas. We use specialized high-resolution subsurface imaging to document active faulting in San Pablo Bay. Near-surface observations are integrated with remote sensing of crustal properties (density and magnetization) and deformation modeling to determine the geometry and connectivity of the Hayward and Rodgers Creek faults.

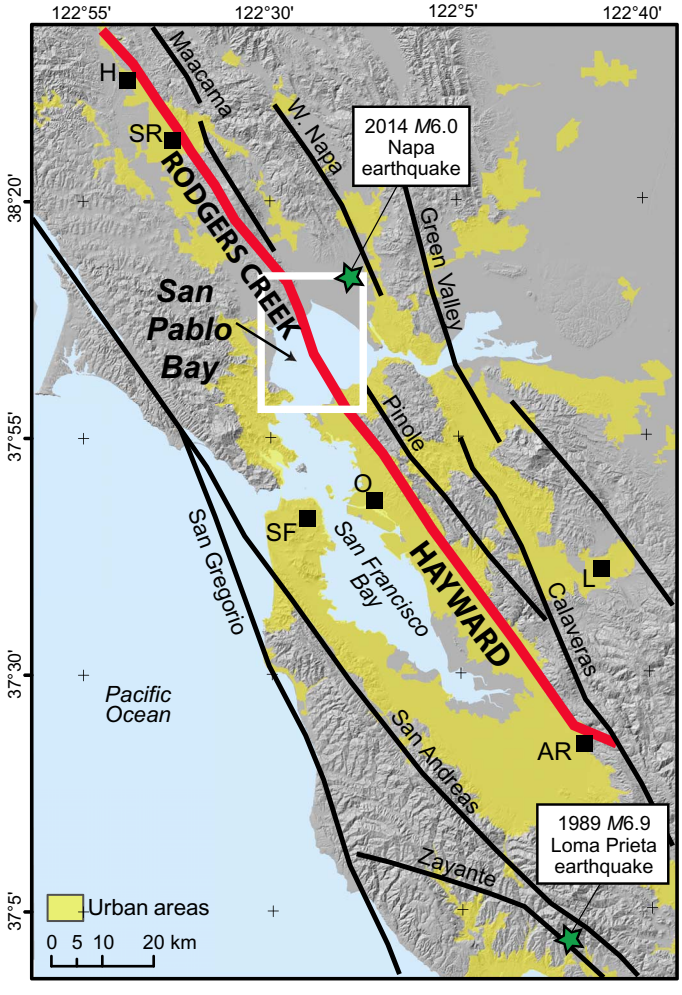

Fig. 1. Map of the Hayward-Rodgers Creek fault zone in the San Francisco Bay Area. Extent of the Hayward-Rodgers Creek fault zone shown in red (*1*, *2*). Black lines show other major faults (*23*, *44*). White box shows study area. Cities are marked with letters: AR, Alum Rock; H, Healdsburg; L, Livermore; O, Oakland; SF, San Francisco; SR, Santa Rosa.

[1]U.S. Geological Survey, Santa Cruz, CA 95060, USA. [2]U.S. Geological Survey, Menlo Park, CA 94025, USA.
*Corresponding author. Email: jwatt@usgs.gov

RESULTS AND DISCUSSION

We acquired ultrahigh-resolution seismic-reflection cross sections (Fig. 2, inset) of the shallow subseafloor across the previously inferred Hayward and Rodgers Creek faults using a chirp subbottom profiler, which uses a high-frequency sound source capable of resolving centimeter-scale deformation of subsurface strata (*16*). Although the presence of free gas within the bay sediments obscures imaging below ~5 m subbottom, these profiles provide clear evidence of near-surface faulting along the Hayward fault beneath the bay. Offset and warping of near-surface sedimentary strata on 13 consecutive seismic profiles delineate a previously unrecognized, northwest-trending strand of the Hayward fault that extends across San Pablo Bay (Fig. 2). As the fault traverses the bay, it gently bends ~10° to the right toward the Rodgers Creek fault. Vertical displacement in the upper 2 to 5 m below the seafloor, as estimated by vertical separation of seismic reflectors, is very small (up to 20 cm). Where cross-fault correlations can be made, offset is predominantly down to northeast (Fig. 3, A to C), with exception of the southernmost profile (Fig. 3D), where offset is down to southwest. Horizontal offsets along the fault are likely to be much larger; however, we were unable to directly measure lateral displacement with these data. The offshore fault strand is presently active because it offsets reflectors near the seafloor (Fig. 3) and it is associated with seismicity (Fig. 2, inset). These new data represent the first direct evidence of active faulting along the offshore extension of the Hayward fault and also provide a framework for evaluating event-scale processes, somewhat akin to paleoseismic trenches onshore.

The shallow deformation observed along the fault may be the result of either coseismic slip (associated with a surface-rupturing earthquake), interseismic creep, or a combination of the two. In San Pablo Bay, there is a distinct along-strike surface creep rate gradient between 5.4 mm/year

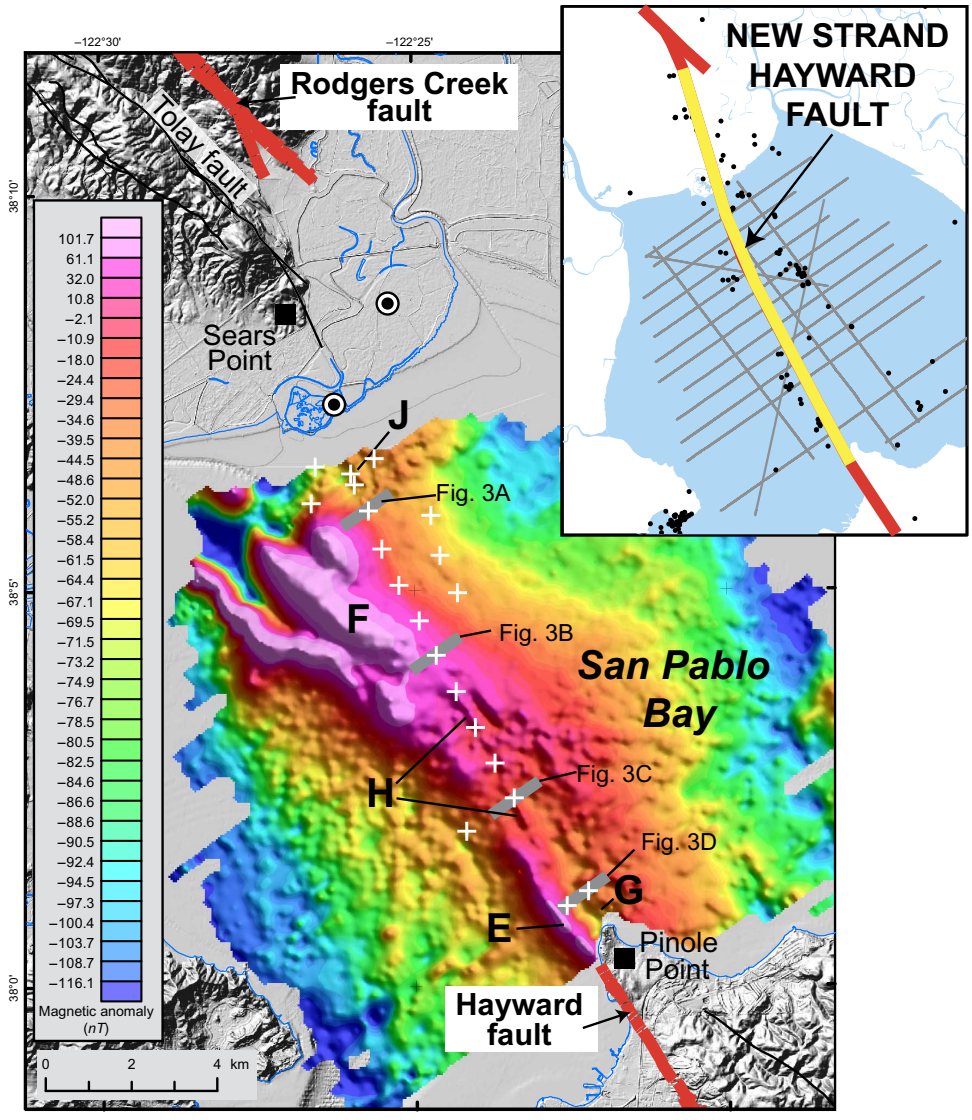

Fig. 2. Marine magnetic map of San Pablo Bay. Warm colors show magnetic highs, and cool colors show magnetic or dipole lows. Plus signs show locations of the offshore Hayward fault along chirp seismic profiles. Thick red lines show Late Pleistocene and younger traces of Hayward and Rodgers Creek faults (*23*). Black lines are older Quaternary faults (*23*). Thick gray lines show locations of seismic profiles in Fig. 3. Capital letters E, F, G, H, and J are discussed in the text. Black circles show exploratory well locations (*5*). Base map, 2010 (1 m) National Oceanic and Atmospheric Administration Lidar. Inset: New Hayward fault strand (yellow) connecting directly to the Rodgers Creek fault. Gray lines show locations of chirp seismic track lines. Small black circles show relocated earthquakes (*22*).

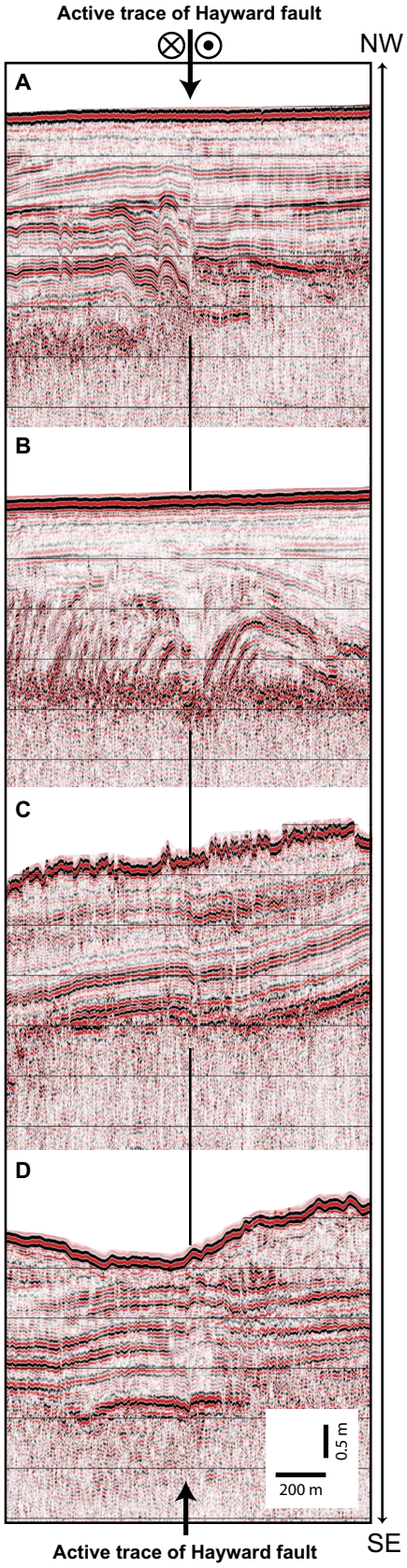

Fig. 3. Chirp seismic profiles along the offshore Hayward fault. (**A**) to (**D**) are discussed in the text. Note vertical exaggeration of ~195:1. NW, northwest; SE, southeast.

along the northern Hayward fault and 1.5 mm/year along the southern Rodgers Creek fault (*17*). Although there are no observations of surface creep in San Pablo Bay, repeating earthquakes identified along the offshore Hayward fault trend (*18*) suggest that seismic Creep is occurring along it.

The offshore strand of the Hayward fault imaged in seismic profiles corresponds to distinct marine magnetic anomaly gradients in the bay, providing evidence that the near-surface fault extends to depth. Marine magnetic data were collected along closely spaced (200 m apart) profiles (*19*), resulting in a high-resolution magnetic map of San Pablo Bay (Fig. 2), where gradients in the magnetic map generally reflect lateral variations in the amount of magnetite in rocks of the upper and middle crust. Locations of gradient maxima denote vertical or near-vertical boundaries of magnetic source rocks. In San Pablo Bay, magnetic source rocks may include a combination of serpentinite, Coast Range Ophiolite, and Tertiary volcanic rocks. The anomaly wavelength is related to the depth of the magnetic source, with long-wavelength anomalies (that is, anomaly F in Fig. 2) reflecting deep sources and short-wavelength anomalies (that is, anomalies E, G, H, and J) reflecting shallow sources. As the fault traverses the bay, it follows the northeast boundary of prominent (high-amplitude) magnetic anomalies E and F (Fig. 2). More subtle (short-wavelength, low-amplitude) linear magnetic anomalies G, H, and J (Fig. 2) along the fault likely reflect folding and/or vertical offset of buried (~100 to 500 m subseafloor) Tertiary volcanic rocks within or directly adjacent to the fault zone. The near-surface fault trace is also colocated with steep east-facing gravity (Fig. 4) and tomographic (*6*) gradients. The isostatic gravity gradient maxima highlighted in Fig. 4 results from the juxtaposition of dense Mesozoic basement rocks to the southwest and less dense Tertiary basin fill deposits to the northeast along the Hayward fault zone. Together, these geophysical data suggest that the active near-surface fault identified in the seismic data extends to seismogenic depths as a vertical or steeply northeast dipping structure.

At its southern end, the Rodgers Creek fault (*20*) branches into two faults just north of San Pablo Bay (Fig. 4), with an eastern strand following the main trend of the Rodgers Creek fault and a western strand that diverges (by ~22°) from the main trend (*21*). Chirp seismic data show no definitive evidence for offset in the near surface along the projected eastern trace of the Rodgers Creek fault (Fig. 5) or along the inferred orthogonal normal fault structures (*7*), defining an active stepover basin beneath San Pablo Bay. The lack of shallow subsurface offset does not preclude the existence of these previously mapped structures but instead indicates that, if present, they are inactive or have not produced near-surface slip within the age of the imaged stratigraphic section.

The offshore Hayward fault points toward the western strand of the Rodgers Creek fault along distinct linear gradients in topographic lidar (Fig. 2) and isostatic gravity (Fig. 4). The northwest-southeast–trending lidar lineament runs along the base of the hills northeast of Sears Point (Fig. 2). The shape of the coincident gravity gradient (Fig. 4) suggests a northeast-dipping contact. In addition, drill cores from onshore wells (Figs. 2 and 4) document ~1 km of down to the northeast vertical offset of the top of the Tertiary volcanic sequence. Together, these data strongly suggest that the offshore Hayward fault connects to the western strand of the Rodgers Creek fault through a releasing (extensional) bend in northern San Pablo Bay. Further northward, as our proposed Hayward-Rodgers Creek fault merges with the eastern strand of the Rodgers Creek fault, it bends ~22° to the northwest, forming a restraining (compressional) bend. The transition from a releasing to restraining geometry (double fault bend) is marked by changes in local

topography, as the lowlands northeast of Sears Point give way to more mountainous terrain near the fault intersection.

Although the Hayward and Tolay faults appear to connect in map view (Fig. 4), geologic map relations (*8*) preclude major strike-slip offset along the Tolay fault since the deposition of the Roblar Tuff (6.26 million years ago). In addition, there is no definitive evidence for Quaternary offset along this fault (*20*), and geologic mapping at their intersection (*8*) shows that the imbricate thrust faults of the Tolay fault are cross-cut by near-vertical faults with northeast-side-down offset. On the basis of the integrated geophysical, geologic, and morphologic evidence for active faulting and structural continuity described above, we conclude that the Hayward and Rodgers Creek faults are directly connected at the surface north of San Pablo Bay (Fig. 5, inset).

KINEMATIC MODELING

To test this assertion, we examine the kinematic implications of direct connectivity between the Hayward and Rodgers Creek faults with deformation models of both disconnected and throughgoing vertical fault geometries (Fig. 6). The models have continuously slipping faults that cause seismic and aseismic deformation to be included implicitly. We compare model-predicted stress patterns with observations of fault deformation and seismicity (*22*).

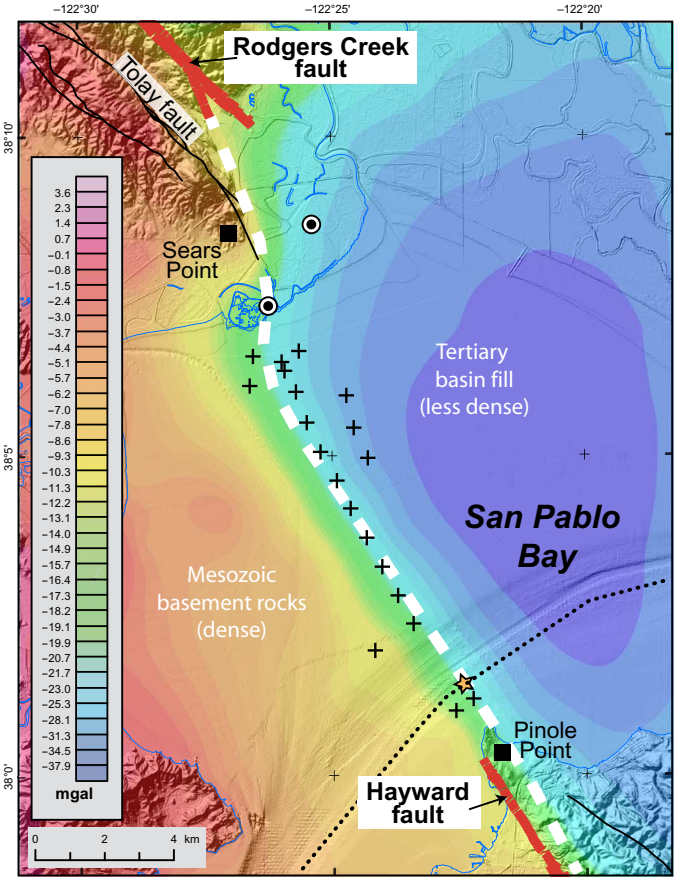

Fig. 4. Isostatic gravity map of San Pablo Bay. Map shows isostatic gravity anomalies in San Pablo Bay (*45*–*47*). Thick dashed white line shows the location of the horizontal gravity gradient maxima relative to the location of the Hayward fault (black plus signs). Orange star shows the location of a steep tomographic gradient along a seismic velocity profile (dotted black line) (*6*).

Acknowledging that our onshore evidence for active faulting is not as strong as the offshore, we construct a disconnected fault model (Fig. 6A) based only on the extent of near-surface offshore faulting and onshore mapped Quaternary active faults (*23*). The relatively short duration [5 ky (thousand years)] of this model run is not meant to simulate long-term deformation but rather to show focused stress/strain that might drive new fault formation. The disconnected fault model (Fig. 6A) forecasts concentrated horizontal shear stress (a proxy for strike-slip faulting) within a north-northwest–south-southeast corridor between the offshore Hayward and the southern Rodgers Creek faults, in agreement with morphological and geophysical indications of faulting onshore.

Figure 6B represents our throughgoing fault bend model based on all available data. The longer duration (100 ky) of this simulation includes multiple earthquake cycles and thus averages the periods over which pre- and postseismic transient deformation takes place. The zone of greatest subsidence predicted in the throughgoing fault model (Fig. 6B) is consistent with off-fault deformation observed along the seismic profiles in the northern half of the bay. Here, seismic profiles reveal a subtle 2- to 3-km-wide elongate depression (Figs. 5 and 6B) along the Hayward fault, indicative of a "lazy Z" (*24*) basin forming within a fault bend. Also, secondary faulting and diffuse seismicity are coincident with areas anticipated to accommodate active extension (Fig. 6B). Agreement between predicted stress patterns and observed deformation reinforces the conclusion that the Hayward and Rodgers Creek faults are directly connected through a fault bend. This geometric relationship has significant implications for seismic hazard and earthquake dynamics.

IMPLICATIONS AND CONCLUSIONS

Current earthquake rupture forecast models for California (*25*) consider the Hayward and Rodgers Creek faults as separate segments that are capable of rupturing together. The discovery of a fault strand directly linking the Hayward and Rodgers Creek faults is particularly noteworthy because this facilitates a simultaneous rupture of the Hayward and Rodgers Creek faults (*12*, *13*, *26*, *27*), potentially producing an earthquake of up to $M = 7.4$ (*28*). This moment magnitude represents the maximum estimate and is a function of fault length and width (*29*), as well as a seismogenic-scaling factor, R, to account for creep along the Hayward fault (*30*). To provide context, an event of $M = 7.4$ would release more than five times the energy as the 1989 $M6.9$ Loma Prieta earthquake (Fig. 1) that caused 63 deaths and an estimated $6 billion to $10 billion in property loss. It is important to remember that the Loma Prieta earthquake was located outside the urban San Francisco Bay Area, and therefore, the damage and loss of life from a similar magnitude earthquake centered within the Bay Area would certainly be much greater.

The occurrence of large multifault earthquakes ($M > 7$) along strike-slip plate boundaries (*12*, *14*) has drawn focus to the influence of fault bends on earthquake physics and ground motion. Dynamic earthquake simulations show that extensional strike-slip fault bends, such as those documented in this study, can promote rupture propagation and amplify ground motions (*13*, *14*). In particular, the detailed geologic structure within fault bends affects the ability of earthquakes to propagate through these discontinuities (*15*). Estimates of shaking intensity from a $M7.2$ simultaneous Hayward-Rodgers Creek scenario earthquake nucleating in San Pablo Bay (*31*) showed the widespread distribution of very strong ground motions throughout the San Francisco Bay Area and particularly within shallow basins

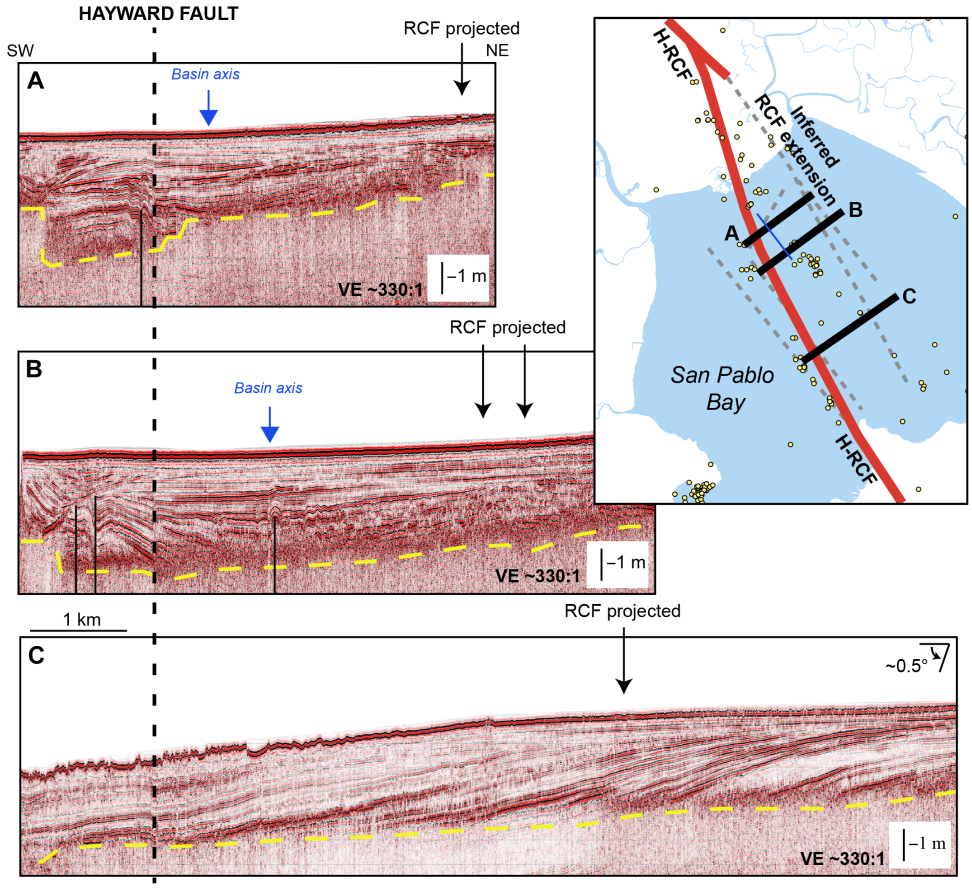

Fig. 5. Seismic profiles illustrating subtle on- and off-fault deformation along the offshore Hayward fault in San Pablo Bay. (**A** to **C**) Seismic profiles and extended views of corresponding profiles **A** and **C** in Fig. 3. Note the presence of an elongate depression (blue arrows) along the Hayward fault in the northern portion of the bay. Black arrows mark the inferred location of the Rodgers Creek fault (RCF). Dashed black line shows location of Hayward fault. Thin black lines indicate older or subsidiary fault structures. Yellow dashed line shows the upper limit of subsurface gas layer. Note vertical exaggeration of ~330:1. Inset: Map of Hayward-Rodgers Creek fault (H-RCF, red line) showing location of seismic profiles A to C (thick black lines). Blue line shows axis of depression along Hayward fault. Gray dashed lines show the previously inferred (*4*, *6*) locations of the Hayward and Rodgers Creek faults in San Pablo Bay. Yellow circles show relocated earthquakes (*22*). SW, southwest; NE, northeast.

beneath the cities of Santa Rosa, Livermore, and San Jose (Fig. 1). However, this scenario was based on what was then considered to be an unlinked stepover and given the documented sensitivity of near-field ground motions to 3D fault geometry (*14*); ground motions in a linked scenario may be considerably different.

In evaluating the potential for cascading rupture along the linked Hayward-Rodgers Creek fault, we must take into consideration that the path an earthquake rupture takes depends not only on fault geometry and connectivity but also on other factors, including earthquake history, stress imparted by past events, and the amount and distribution of creep occurring along the faults (*10*, *12*, *17*, *32*). Geodetic and paleoseismic evidence (*17*, *28*, *33*, *34*) indicates that the Hayward and Rodgers Creek faults have each accumulated enough stress to produce a large earthquake. In addition, stress along the southern Rodgers Creek and northern Hayward faults may be elevated as a result of static Coulomb stress changes resulting from the nearby 2014 *M*6 Napa earthquake (Fig. 1) (*35*). Estimates of the timing of the most recent event along the Rodgers Creek fault and prehistoric events along the Hayward fault allow the possibility of a combined rupture between 1715 CE and 1776 CE (*2*, *28*). However, differences in fault frictional properties between creeping and locked segments along the Hayward-Rodgers Creek fault may inhibit cascading ruptures (*17*, *32*), with the exception of large earthquakes originating on the Rodgers Creek fault (*17*, *36*). Currently, the distribution of frictional properties along the Hayward fault beneath San Pablo Bay and along the southern Rodgers Creek fault is very poorly constrained, and therefore, future studies focused on characterizing the fault behavior and earthquake history of these areas may provide valuable insight into the potential for throughgoing rupture.

Distinguishing and characterizing presently active structures within structurally complex and dynamic strike-slip fault bends is vital for understanding the physics of large cascading ruptures and forecasting their future occurrence. Active deformation within fault steps or bends is often subtle (centimeter-scale) and/or distributed, where individual faults may be blind and/or obscured by surface processes. This work and similar structural investigations of fault bends and stepovers (*1*, *2*, *12*, *37*, *38*) highlight the importance of integrative and multiscale geologic/geophysical investigations at fault discontinuities for comprehensively documenting fault deformation and providing fundamental science for achieving earthquake resilience.

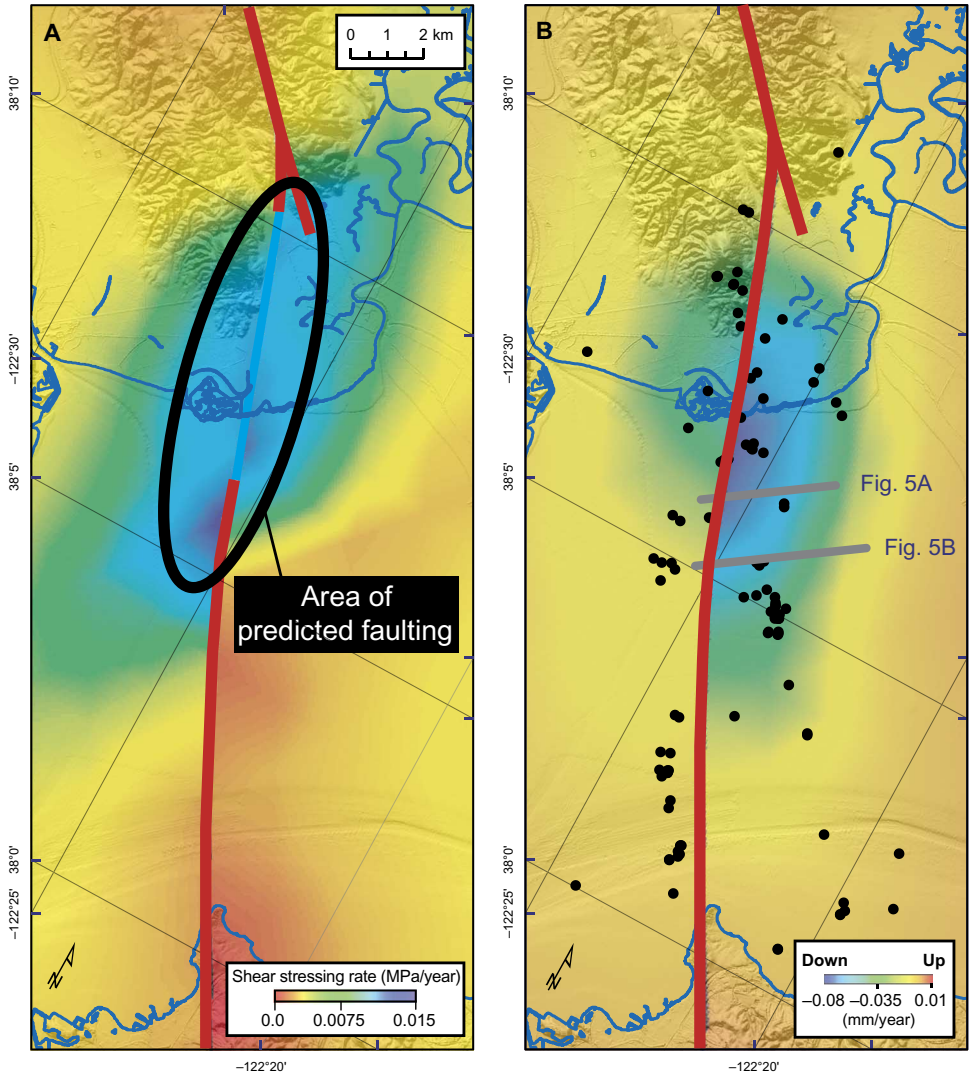

Fig. 6. Kinematic finite element models of the Hayward-Rodgers Creek fault in San Pablo Bay. (**A**) Model showing the predicted magnitude of horizontal shear stress after 5 ky of slip [9 mm/year (*25*)] along a disconnected Hayward-Rodgers Creek fault (red line). The model fault is relieving stress continually, except at fault endpoints. (**B**) Through-going fault model showing predicted vertical deformation after 100 ky of slip. Gray lines indicate locations of seismic profiles shown in Fig. 5. See Materials and Methods for detailed description of model methods and parameters.

MATERIALS AND METHODS

Here, we used a combination of specialized high-resolution geophysical techniques to image the shallow structure beneath San Pablo Bay. We collected approximately 200 line-km of seismic reflection data along northeast- and northwest-trending profiles (Fig. 2, inset) spaced 1 km apart using an Edgetech 512 chirp subbottom profiler that was towed alongside the vessel on a sled at the sea surface (*16*). Data were acquired using a 2- to 12-kHz sweep, with a 20-ms length fired six times per second. Processing included subsampling at twice the sample interval, static corrections, predictive deconvolution, and trace mixing. Because of attenuation of the chirp signal by bay mud and persistent natural gas layers in San Pablo Bay sediments, we were only able to image the upper 2 to 5 m of the subseafloor. Vertical accuracy of the data is approximately 5 cm.

In addition, more than 1200 line-km of shipborne magnetometer data were collected along traverses oriented similarly to the seismic reflection data, with profiles spaced 200 m apart using a Geometrics G-858 cesium vapor magnetometer attached to a pole extended about 2 m in front of the ship's bow (*19*). Data were collected at 0.1-s intervals, resulting in an average station spacing of 0.5 m. Corrections were made to remove the effects due to vessel heading, diurnal variations, and the regional field (International Geomagnetic Reference Field). Data were gridded to 50 m for interpretation (Fig. 2).

The 3D finite element models in Fig. 6 were constructed using the commercial ANSYS code and were intended to estimate near-surface and near-fault stress and deformation implied by geophysical observations. The range of possible models includes those with slipping fault terminations, which, if embedded in an elastic representation of the crust, can introduce stress singularities at the fault tips. Therefore, we used element fracturing and accompanying plastic deformation to enable the model crust to deform at scales that are consistent with real-world observations.

The elastic/plastic upper crust was modeled using eight-node (including midside nodes), breakable tetrahedral elements. The physical properties of the upper crust were taken from measurements on fully saturated Westerly granite and were described by four elastic constants: Young's modulus ($E = 8.0 \times 10^4$ MPa), density ($\rho = 2.7 \times 10^3$ kg^3 m^{-3}), Poisson's ratio ($\lambda = 0.25$), and an internal friction coefficient (*39*–*41*). The elastic/plastic elements were engineered by ANSYS to replicate rock behavior; the elements behave elastically up to a critical stress level and then exhibit permanent deformation through cracking. This happens when the defined strength of the element is overcome by the calculated differential stress magnitude. Failure occurs on planes defined by the stress tensor and coefficient of internal friction for granite.

Crack formation is characterized by changing the solved-for stress-strain relation in a direction that is orthogonal to the crack. Strength reduction comes from loading, which induces sliding on the crack plane. Multiple cracks can occur in response to evolving stress orientations. This process is calculated using the Willam-Warnke failure criterion for three nontensional principal stresses (*42*). The models were rotated so that the edges are parallel and orthogonal to the best linear fit to the trend of the faults. The top of the model was unconstrained (free surface) and started out with no relief. The eastern edges were fixed, and the western edges were slipped at 9 mm/year (*25*) to cause continuous fault slip. The model base was set to the maximum seismogenic depth of 15 km (*25*) and could move horizontally (without frictional resistance) but not vertically. No other limits were prescribed other than gravitational loading. We assumed that preseismic transient deformation was balanced by coseismic slip and postseismic accommodation (*43*). No deep after-slip or upper mantle postseismic effects were modeled explicitly. Primary testable model results of interest are the expected vertical displacements and stress concentrations that result from fault slip.

REFERENCES AND NOTES

1. E. Chaussard, R. Bürgmann, H. Fattahi, R. M. Nadeau, T. Taira, C. W. Johnson, I. Johanson, Potential for larger earthquakes in the East San Francisco Bay Area due to the direct connection between the Hayward and Calaveras Faults. *Geophys. Res. Lett.* **42**, 2734–2741 (2015).
2. S. Hecker, V. E. Langenheim, R. A. Williams, C. S. Hitchcock, S. B. DeLong, Detailed mapping and rupture implications of the 1 km releasing bend in the Rodgers Creek fault at Santa Rosa, Northern California. *Bull. Seismol. Soc. Am.* **106**, 575–594 (2016).
3. E. H. Field, G. P. Biasi, P. Bird, T. E. Dawson, K. R. Felzer, D. D. Jackson, K. M. Johnson, T. H. Jordan, C. Madden, A. J. Michael, K. R. Milner, M. T. Page, T. Parsons, P. M. Powers, B. E. Shaw, W. R. Thatcher, R. J. Weldon II, Y. Zeng, Long-term time-dependent probabilities for the Third Uniform California Earthquake Rupture Forecast (UCERF3). *Bull. Seismol. Soc. Am.* **105**, 511–543 (2015).
4. T. L. Wright, N. Smith, Right step from the Hayward fault to the Rodgers Creek fault beneath San Pablo Bay. *Div. Mines Geol. Spec. Publ.* **113**, 407–417 (1992).
5. R. C. Jachens, C. M. Wentworth, M. L. Zoback, T. R. Bruns, C. W. Roberts, Concealed strands of the San Andreas fault system in central San Francisco Bay Region, as inferred from aeromagnetic anomalies. *U.S. Geol. Surv. Profess. Pap.* **1658**, 43–61 (2002).
6. T. Parsons, R. Sliter, E. L. Geist, R. C. Jachens, B. E. Jaffe, A. Foxgrover, P. E. Hart, J. McCarthy, Structure and mechanics of the Hayward–Rodgers Creek fault step-over, San Francisco Bay, California. *Bull. Seismol. Soc. Am.* **93**, 2187–2200 (2003).
7. R. W. Graymer, A. M. Sarna-Wojcicki, J. P. Walker, R. J. McLaughlin, R. J. Fleck, Controls on timing and amount of right-lateral offset on the East Bay fault system, San Francisco Bay region, California. *Geol. Soc. Am. Bull.* **114**, 1471–1479 (2002).
8. D. L. Wagner, G. J. Saucedo, K. B. Clahan, R. J. Fleck, V. E. Langenheim, R. J. McLaughlin, A. M. Sarna-Wojcicki, J. R. Allen, A. L. Deino, Geology, geochronology, and paleogeography of the southern Sonoma volcanic field and adjacent areas, northern San Francisco Bay region, California. *Geosphere* **7**, 658–683 (2011).
9. J. J. Lienkaemper, G. Borchardt, M. Lisowski, Historic creep rate and potential for seismic slip along the Hayward Fault, California. *J. Geophys. Res.* **96**, 18261–18283 (1991).
10. J. J. Lienkaemper, F. S. McFarland, R. W. Simpson, R. G. Bilham, D. A. Ponce, J. J. Boatwright, S. J. Caskey, Long-term creep rates on the Hayward fault: Evidence for controls on the size and frequency of large earthquakes. *Bull. Seismol. Soc. Am.* **102**, 31–41 (2012).
11. S. G. Wesnousky, Predicting the endpoints of earthquake ruptures. *Nature* **444**, 358–360 (2006).
12. D. P. Schwartz, P. J. Haeussler, G. G. Seitz, T. E. Dawson, Why the 2002 Denali fault rupture propagated onto the Totschunda fault: Implications for fault branching and seismic hazards. *J. Geophys. Res.* **117**, B11304 (2012).
13. J. C. Lozos, D. D. Oglesby, B. Duan, S. G. Wesnousky, The effects of double fault bends on rupture propagation: A geometrical parameter study. *Bull. Seismol. Soc. Am.* **101**, 385–398 (2011).
14. D. D. Oglesby, P. M. Mai, Fault geometry, rupture dynamics and ground motion from potential earthquakes on the North Anatolian Fault under the Sea of Marmara. *Geophys. J. Int.* **188**, 1071–1087 (2012).
15. Y. Finzi, S. Langer, Damage in step-overs may enable large cascading earthquakes. *Geophys. Res. Lett.* **39**, L16303 (2012).
16. J. T. Watt, P. E. Hart, J. W. Kluesner, *Chirp Seismic-Reflection Data: San Pablo Bay, California* (U.S. Geological Survey, 2016).
17. J. J. Lienkaemper, F. S. McFarland, R. W. Simpson, S. J. Caskey, Using surface creep rate to infer fraction locked for sections of the San Andreas fault system in northern California from alignment array and GPS data. *Bull. Seismol. Soc. Am.* **104**, 3094–3114 (2014).
18. M. Shirzaei, R. Bürgmann, Time-dependent model of creep on the Hayward fault from joint inversion of 18 years of InSAR and surface creep data. *J. Geophys. Res.* **118**, 1733–1746 (2013).
19. D. A. Ponce, K. M. Denton, J. T. Watt, *Marine Magnetic Survey and Onshore Gravity and Magnetic Survey, San Pablo Bay, Northern California* (U.S. Geological Survey, 2016).
20. R. J. McLaughlin, A. M. Sarna-Wojcicki, D. L. Wagner, R. J. Fleck, V. E. Langenheim, R. C. Jachens, K. Clahan, J. R. Allen, Evolution of the Rodgers Creek–Maacama right-lateral fault system and associated basins east of the northward-migrating Mendocino Triple Junction, northern California. *Geosphere* **8**, 342–373 (2012).
21. E. W. Hart, *Recently Active Traces of the Rodgers Creek Fault, Sonoma County, California* (California Division of Mines and Geology, 1992).
22. F. Waldhauser, D. P. Schaff, Large-scale relocation of two decades of Northern California seismicity using cross-correlation and double-difference methods. *J. Geophys. Res.* **113**, B08311 (2008).
23. U.S. Geological Survey (USGS) and California Geological Survey, *Quaternary Fault and Fold Database of the United States* (USGS, 2010); http://earthquake.usgs.gov/hazards/qfaults/.
24. P. Mann, Global catalogue, classification, and tectonic origin of restraining and releasing bends on active and ancient strike-slip fault systems, in *Tectonics of Strike-slip Restraining and Releasing Bends,* W. D. Cunningham, P. Mann, Eds. (Geological Society, London, Special Publication, 2007), vol. 290, pp. 13–142.
25. E. H. Field, R. J. Arrowsmith, G. P. Biasi, P. Bird, T. E. Dawson, K. R. Felzer, D. D. Jackson, K. M. Johnson, T. H. Jordan, C. Madden, A. J. Michael, K. R. Milner, M. T. Page, T. Parsons, P. M. Powers, B. E. Shaw, W. R. Thatcher, R. J. Weldon II, Y. Zeng, Uniform California Earthquake Rupture Forecast, version 3 (UCERF3)—The time-independent model. *Bull. Seismol. Soc. Am.* **104**, 1122–1180 (2014).
26. H. Magistrale, S. Day, 3D simulations of multi-segment thrust fault rupture. *Geophys. Res. Lett.* **26**, 2093–2096 (1999).
27. D. D. Oglesby, The dynamics of strike-slip step-overs with linking dip-slip faults. *Bull. Seismol. Soc. Am.* **95**, 1604–1622 (2005).
28. D. P. Schwartz, J. J. Lienkaemper, S. Hecker, K. I. Kelson, T. E. Fumal, J. N. Baldwin, G. G. Sietz, T. M. Niemi, The earthquake cycle in San Francisco Bay region: A.D. 1600–2012. *Bull. Seismol. Soc. Am.* **104**, 1299–1328 (2014).
29. T. C. Hanks, W. H. Bakun, M-log*A* observations for recent large earthquakes. *Bull. Seismol. Soc. Am.* **98**, 490–494 (2008).
30. Working Group on California Earthquake Probabilities, *Earthquake Probabilities in the San Francisco Bay Region: 2002–2031* (U.S. Geological Survey, 2003).
31. B. T. Aagaard, R. W. Graves, A. Rodgers, T. M. Brocher, R. W. Simpson, D. Dreger, N. A. Peterson, S. C. Larsen, S. Ma, R. C. Jachens, Ground-motion modeling of Hayward fault scenario earthquakes, part II: Simulation of long-period and broadband ground motions. *Bull. Seismol. Soc. Am.* **100**, 2945–2977 (2010).
32. J. C. Lozos, R. A. Harris, J. R. Murray, J. J. Lienkaemper, Dynamic rupture models of earthquakes on the Bartlett Springs Fault, Northern California. *Geophys. Res. Lett.* **42**, 4343–4349 (2015).
33. J. J. Lienkaemper, P. L. Williams, T. P. Guilderson, Evidence for a twelfth large earthquake on the southern Hayward fault in the past 1900 years. *Bull. Seismol. Soc. Am.* **100**, 2024–2034 (2010).
34. S. Hecker, D. Pantosti, D. P. Schwartz, J. C. Hamilton, L. M. Reidy, T. J. Powers, The most recent large earthquake on the Rodgers Creek fault, San Francisco Bay area. *Bull. Seismol. Soc. Am.* **95**, 844–860 (2005).

35. T. Parsons, M. Segou, V. Sevilgen, K. Milner, E. Field, S. Toda, R. S. Stein, Stress-based aftershock forecasts made within 24h postmain shock: Expected north San Francisco Bay area seismicity changes after the 2014 *M*=6.0 West Napa earthquake. *Geophys. Res. Lett.* **41**, 1–8 (2014).
36. H. Noda, N. Lapusta, Stable creeping fault segments can become destructive as a result of dynamic weakening. *Nature* **493**, 518–521 (2013).
37. J. T. Watt, D. A. Ponce, R. W. Graymer, R. C. Jachens, R. W. Simpson, Subsurface geometry of the San Andreas-Calaveras fault junction: Influence of serpentinite and the Coast Range Ophiolite. *Tectonics* **33**, 2025–2044 (2014).
38. R. W. Graymer, V. E. Langenheim, R. W. Simpson, R. C. Jachens, D. A. Ponce, Relatively simple through-going fault planes at large-earthquake depth may be concealed by the surface complexity of strike-slip faults, in *Tectonics of Strike-slip Restraining and Releasing Bends*, W. D. Cunningham, P. Mann, Eds. (Geological Society, London, Special Publication, 2007), vol. 290, pp. 189–201.
39. F. Birch, Compressibility: Elastic constants. *Geol. Soc. Am. Mem.* **97**, 97–174 (1966).
40. J. Byerlee, Friction of rocks. *Pure Appl. Geophys.* **116**, 615–626 (1978).
41. N. I. Christensen, Poisson's ratio and crustal seismology. *J. Geophys. Res.* **101**, 3139–3156 (1996).
42. K. J. Willam, E. P. Warnke, Constitutive models for the triaxial behavior of concrete. *Proc. Int. Assoc. Bridge Struc. Eng.* **19**, 1–30 (1974).
43. B. J. Meade, Y. Klinger, E. A. Hetland, Inference of multiple earthquake-cycle relaxation timescales from irregular geodetic sampling of interseismic deformation. *Bull. Seismol. Soc. Am.* **103**, 2824–2835 (2013).
44. V. E. Langenheim, R. W. Graymer, R. C. Jachens, R. J. McLaughlin, D. L. Wagner, D. S. Sweetkind, Geophysical framework of the northern San Francisco Bay region, California. *Geosphere* **6**, 594–620 (2010).
45. D. A. Ponce, *Principal Facts for Gravity Data Along the Hayward Fault and Vicinity, San Francisco Bay Area, Northern California* (U.S. Geological Survey, 2001).
46. V. E. Langenheim, C. W. Roberts, C. A. McCabe, D. K. McPhee, J. E. Tilden, R. C. Jachens, *Preliminary Isostatic Gravity Map of the Sonoma Volcanic Field, Sonoma and Napa Counties, Northern California* (U.S. Geological Survey, 2006).
47. R. W. Simpson, R. C. Jachens, R. C. Saltus, R. J. Blakely, *Isostatic Residual Gravity, Topographic, and First-Vertical Derivative Gravity Maps of the Conterminous United States* (U.S. Geological Survey, 1986).

Acknowledgments: We would like to thank K. Denton, J. White, P. Dal Ferro, J. Currie, B. Chuchel, C. McPherson-Krutsky, and K. Morgan of the U.S. Geological Survey (USGS) for their assistance in field data collection efforts and D. Brubaker and M. Amato at the San Pablo Bay National Wildlife Refuge for providing key logistical field support and property contacts for the area. This work benefited from discussions with D. Brothers, R. Graymer, S. Hecker, S. Johnson, J. Lienkaemper, V. Langenheim, D. Schwartz, D. Wagner, and T. Wright. We appreciate the critical seismic processing support provided by J. Kluesner of the USGS. We also thank K. Fischer, D. Schwartz, and two anonymous reviewers for their thoughtful and constructive comments that greatly improved this manuscript. **Funding:** This work was supported by the USGS National Earthquake Hazards and Coastal and Marine Geology Programs, as well as the USGS Pacific Region. **Author contributions:** J.W. and D.P. collaboratively proposed and oversaw this project, and J.W. prepared the majority of the manuscript. D.P. was responsible for collection and processing of marine magnetic data, and both J.W. and D.P. conducted geologic interpretation. J.W. and P.H. were responsible for collection and processing of the seismic reflection data, and J.W. conducted all geologic interpretation. T.P. was responsible for deformation modeling, with structural input provided by J.W. All authors contributed to the final manuscript. **Competing interests:** The authors declare that they have no competing interests. **Data and materials availability:** All raw and processed seismic profiles are available in .segy format online in ScienceBase (*16*). Marine magnetic data are available online as a USGS open-file report (*19*). All other gravity, magnetic, well, and seismicity data used in this study are publicly available (see citations in text). Additional data related to this paper may be requested from the authors.

Submitted 24 June 2016
Accepted 22 September 2016
Published 19 October 2016
10.1126/sciadv.1601441

Citation: J. Watt, D. Ponce, T. Parsons, P. Hart, Missing link between the Hayward and Rodgers Creek faults. *Sci. Adv.* **2**, e1601441 (2016).